Journal of Colloid and Interface Science 476 (2016) 20–28

Contents lists available at ScienceDirect

Journal of Colloid and Interface Science

journal homepage: www.elsevier.com/locate/jcis

# Stray-field NMR diffusion *q*-space diffraction imaging of monodisperse coarsening foams

Kieron Smith [a], Adam Burbidge [b], David Apperley [a], Paul Hodgkinson [a], Fraser A. Markwell [a], Daniel Topgaard [c], Eric Hughes [a,*]

[a] Department of Chemistry, Durham University, South Road, Durham DH1 3LE, UK
[b] Nestle Research Centre, Nestec Ltd. Vers-chez-les-Blanc, Case Postale 44, 1000 Lausanne 26, Switzerland
[c] Division of Physical Chemistry, Department of Chemistry, Lund University, SE-221 00 Lund, Sweden

## GRAPHICAL ABSTRACT

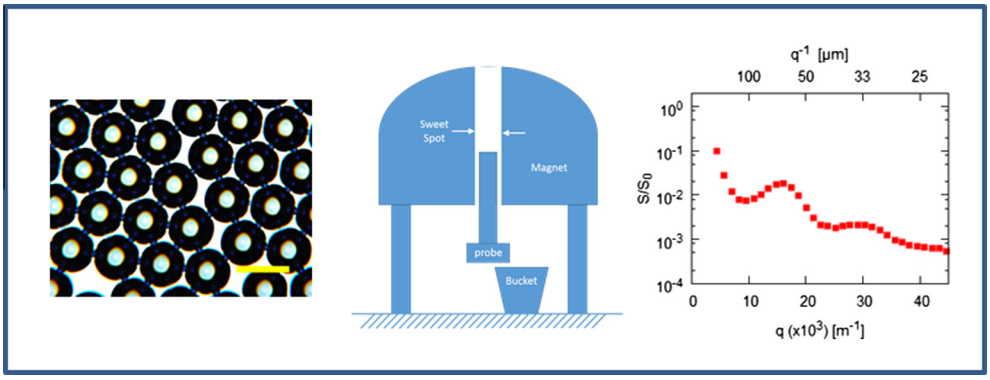


## ARTICLE INFO

*Article history:*
Received 15 December 2015
Revised 28 April 2016
Accepted 28 April 2016
Available online 6 May 2016

*Keywords:*
Monodisperse
Foam
Stray field
NMR
Diffraction
Diffusion
Coarsening
Relaxation

## ABSTRACT

The technique of stray field diffusion NMR is adapted to study the diffusion properties of water in monodisperse wet foams. We show for the first time, that the technique is capable of observing *q*-space diffusion diffraction peaks in monodisperse aqueous foams with initial bubble sizes in the range of 50–85 μm. The position of the peak maximum can be correlated simply to the bubble size in the foam leading to a technique that can investigate the stability of the foam over time.

The diffusion technique, together with supplementary spin-spin relaxation analysis of the diffusion data is used to follow the stability and coarsening behaviour of monodisperse foams with a water fraction range between 0.24 and 0.33. The monodisperse foams remain stable for a period of hours in terms of the initial bubble size. The duration of this stable period correlates to the initial size of the bubbles. Eventually the bubbles begin to coarsen and this is observed in changes in the position of the diffusion diffraction maxima.



## 1. Introduction

Aqueous foams are of commercial importance in the food, cosmetic and personal health-care industries [1] and therefore attract

* Corresponding author.
*E-mail address:* eric.hughes@dur.ac.uk (E. Hughes).

http://dx.doi.org/10.1016/j.jcis.2016.04.053
0021-9797/

a lot of research interest. Much of the research involves understanding and improving the stability of the foams in terms of drainage, coalescence and coarsening [2,3]. All three processes can occur simultaneously, each one influencing the other, leading quickly to a destabilised foam. This makes it difficult experimentally to isolate and study the main destabilising processes occurring in a particular foam. A number of studies have resorted to monodispersed foams confined to one and two dimensions [4–6] to reduce the complexity of the problem while focusing on one or two destabilisation phenomena. Other studies interested in coarsening, have resorted to performing experiments under micro-gravity conditions [7,8] to slow down drainage.

Liquid monodisperse foams can be classified into two broad groups, wet and dry, depending on the percentage of water present in the foam. Foams with a water percentage (water fraction) below 5% (0.05) [4] are classed as dry, the bubbles are deformed and polyhedral in nature, with bubble faces sharing the same interface. Bubbles in wet foams become increasingly spherical in shape as the water fraction increases and above a certain water fraction, the wet limit, the bubbles lose contact with one another. This limit lies between 0.26 and 0.33 depending on whether the monodisperse foams are packed in a crystalline or disordered manner [4,9].

The coarsening of foams, where large bubbles grow at the expense of smaller bubbles due to Laplace pressure differences is of interest at both an academic and industrial level. The coarsening dynamics of dry and wet foams differ as the dominant gas transport mechanism between bubbles is not the same [7,9]. In dry foams the transport of gas is direct, proceeding through the large interfaces between touching bubbles leading to a growth rate of the bubbles proportional to $t^{1/2}$. In wet foams, above the wet limit, the transport of gas is dominated by diffusive properties of the gas in the liquid phase with a growth rate proportional to $t^{1/3}$.

For two-dimensional (2-D) dry foams von-Neumann proposed a simple model for the coarsening of foams based upon the number of faces a bubble possesses [10]. This model has been verified experimentally [11,12], leading to a coarsening phenomena at long times, where the growth rate of the bubbles in the foam becomes self-similar. In three-dimensional (3-D) foams it was not obvious that coarsening behaves in the same manner. Only recently, has an exact von-Neumann-like growth equation been published for dry 3-D foams [13]. Experimental evidence is only now being published based on fast X-ray tomography [14,15] and light scattering techniques using magnetically levitated foams [7,8].

Wet foams with intermediate water fractions between that of dry and the wet limit, are expected to show coarsening dynamics which lie between the two extremes. However, this may not necessarily be the case when other factors such as viscous or inertial hydrodynamics act [16] and growth rates greater than 0.5 are predicted. Therefore, there is scope for applying other physical spectroscopic methods to understand foam stability and dynamics in this water fraction region that are non-invasive and relatively fast. In this paper, nuclear magnetic resonance diffusion experiments are developed to investigate the coarsening behaviour of monodisperse foams with diameters in the range of 50–80 μm and water fractions between 0.24 and 0.33. In this intermediate regime, the bubbles are touching and only slightly deformed from the ideal spherical shape observed at higher water fractions.

### 1.1. NMR background

Magnetic resonance, in its many forms, has been used to study the structure of foams. Magnetic resonance imaging has been used to measure foam drainage [17,18] and structure to give bubble size distribution directly from 3-D data sets for bubble diameters greater than 200 μm [19,20]. More recently, there has been an emphasis on speeding up the experiment time by reducing the image dimensionality and using Bayesian statistical methods to extract the bubble size distribution of a foam [21–23]. This approach has advantages in that the experimental data collection is simple, however, the building and validation of the statistical model can be quite involved.

NMR spin-spin relaxation ($T_2$) data has been used to give the bubble size distribution in a hydrogel foam [24] and the method has been applied to the study of lung microstructure [25] to understand disease. The approach has been developed from NMR studies of porous media [26–28]. The $T_2$ relaxation of a fluid in a porous medium becomes a function of the surface to volume ratio of the pores and diffusion of the liquid in the internal gradients arising from the susceptibility differences at the liquid/solid interface and therefore becomes a probe of the pore structure. The approach requires a number of supporting parameters to be obtained from other methods in order to arrive at a final size distribution.

Self-diffusion NMR has been used extensively with emulsions to give a droplet size distribution of the dispersed phase under conditions of long diffusion observation times where diffusion of the disperse phase is restricted [29]. With foams however, the method used in its traditional manner, requires an NMR active gas to probe the bubble dimensions [30]. The approach has been shown to work using propane gas, but the water signal had to be suppressed using dissolved rare earth ions. Their addition was shown to have an effect on the surface tension of the aqueous phase making the method difficult to use for foam systems where the nature of the aqueous phase cannot be altered.

In dispersed systems, with low polydispersity, self-diffusion NMR has been used to obtain an estimate of the dispersed sphere size. Due to the low polydispersity, $q$-space diffraction peaks [31–33] are observed in the echo decay of the diffusion experiment as a function of increasing gradient strength. The position of the peak maxima occur when the gradient strength, $q$ is equal to the reciprocal of the characteristic dimensions, $b$, of the dispersed phase, such as the diameter of the droplets in a monodisperse emulsion. This method has since been used to investigate systems such as red blood cells [34] to study membrane permeability and low polydisperse emulsions made by hand [35,36] to follow Ostwald ripening [37] and more recently by the use of microfluidics [38–40].

In order to observe the phenomena, the diffusing molecules must be allowed sufficient time so that the majority have explored on average, a distance that is characteristic of the underlying structure. This diffusion time, $\Delta$, is of the order of $b^2/D_0$, where $b$ is the diameter of the dispersed phase in an emulsion or foam and $D_0$ is the free diffusion coefficient of the molecules being observed in the NMR experiment. For droplets of diameter 50 μm, if water is being observed ($D_0 = 2.3 \times 10^{-9}$ m$^2$ s$^{-1}$ at 25 °C) then the diffusion time required is of the order of 1 s. This then requires that the spin lattice relaxation time ($T_1$) of the diffusing molecules be on the order of a few seconds. Typically, in foam and emulsion systems, the water $T_1$ is around 3 s.

Both the dispersed and continuous phase may be used to observe the diffraction phenomena, the choice is dictated by the magnitude of the free diffusion coefficient, the $T_1$ relaxation and characteristic size of the internal structure probed. For the continuous phase to be used, as is required for a foam system, the dispersed phase must be concentrated. Therefore, foams with air to water fractions greater than 30% are required. This makes the technique applicable to dry foams and wet foams up to the point where the bubbles are just touching.

The investigation of monodisperse wet foams with bubble diameters covering the range from 10 to 100 μm, prepared using microfluidic techniques [41–43] should be amenable to this approach. However, the experimental study of wet foams by

$q$-space diffusion NMR is difficult for two reasons: the short life time of the foam and the large internal gradients arising from susceptibility differences from the air water interfaces present.

Aqueous wet foams are thermodynamically unstable and tend to break down with time. NMR diffusion experiments can take over an hour to complete and some foams can destabilize completely within minutes, therefore the use of an insoluble gas to stabilise the foam against coarsening is required [43,44].

The proton spin-spin relaxation time of the water in the foam is altered from its bulk value due to a number of factors. Enhanced relaxation can occur from surface relaxation of molecules colliding with the air water interface. The smaller the size of the bubbles in a foam, the larger the surface to volume ratio, leading to a decrease in the spin-spin relaxation time due to enhanced surface relaxation [24]. Diffusion in the large internal gradients present in the foam leads to the spin-spin relaxation observed via an echo experiment being dependent on the refocusing time. When pulse-field gradient experiments are performed the maximum time allowed for the encoding time, including gradient pulse duration and recovery time, is comparable to the decay time of the free induction decay $(T_2^*)$. The proton NMR line width at half height of a foam in the present study is of the order of 5–10 ppm. At a proton Larmor frequency of 400 MHz, this leads to a line width at half height on the order of 1500 Hz and a FID decay time $(T_2^*)$ of 250–500 μs. Modern commercial dedicated pulsed field gradient probes, capable of producing gradient pulses of 1800 G/cm would struggle to perform with gradient echo times of less than 1 ms when the gradient recovery time is taken into consideration.

In order to overcome these problems, without resorting to modifying the chemical properties of the foam to increase the relaxation times, stray field gradient diffusion techniques [45–47] have been investigated.

Stray field gradient imaging [48] and diffusion studies employ a strong permanent static gradient throughout the experiment pulse sequence, therefore the need for long gradient encoding times is not required. The methodology has been used for imaging at high and low Larmor frequencies using the fringe-field of superconducting magnets or employing specifically designed systems, usually at low magnetic field [49]. In this study we employ the fringe-field of the superconducting NMR magnet. This provides flexibility to choose the strength of the magnetic field gradient, while keeping the sensitivity of the experiment high. Furthermore, the experiment uses standard NMR probes to make the experiment open to non-specialists.

In this paper, we develop the method for investigating foam using stray-field NMR using a number of different probes, validating the method by using a standard sample of polystyrene monodisperse beads. The long term stability of a series of monodisperse foams are investigated using the method together with supplementary $T_2$ relaxation techniques. The results are discussed in terms of the initial size of the foam bubbles, the wetness of the foam and the main destabilization mechanism involved.

## 2. Materials and methods

### 2.1. Materials

Monodisperse 50 μm diameter polystyrene beads (Duke Standards 4250A) surrounded by water were used as a standard to develop the stray-field diffusion methods. The beads were allowed to settle in a Bruker Kel-F 4 mm high resolution magic angle spinning (HR-MAS) insert (Part Number: B4493). The excess water was removed and the process repeated until the insert was full. The sample was then sealed. Distilled water was used as a gradient calibration standard. The sample volume of the insert is cylindrical in shape with an inner diameter of 2.2 mm. The sample length of the insert was then calculated to be 6.8 mm by weighing and averaging a number of inserts filled with water and sealed. The total volume of sample is approximately 27 μL.

A 1 wt% Tween 20 (Polysorbate 20) solution was used to prepare the foam. The stability of the foam was increased by the addition of perfluorohexane (Sigma Aldrich) as a vapour into the gas phase. Foam samples for the NMR experiments were prepared in three different sample holders. A 4 mm HR-MAS insert, the zirconia ceramic 4 mm rotor and a glass 5 mm diameter cut-off NMR tube. The foam was loaded into the NMR sample holders by first filling the holders with surfactant solution and then placing the holder above the output of the microfluidics device and just touching the foam flow being produced. The foam samples were weighed to give an estimate of the volume fraction of water in the sample assuming a density of the surfactant phase of 1 g/mL. Samples of the foam were also collected on a microscope slide before and after filling the sample holder to check the size and monodispersity of the bubbles using a LCD Digital Microscope II (Celestron Torrance CA).

### 2.2. Microfluidics

Monodisperse foam samples were prepared using a home-built microfluidic device published by Stone and co-workers [50] and a commercial flow-focusing microfluidic chip (Part Number: 3000158 Dolomite, Royston UK). The air and liquid flows were controlled using pressure using two Mitos Fluika low pressure pumps (pt.200418). The operating pressure range for the microfluidic devices was between 50 and 500 mbar and the bubble diameter range achievable with the two systems was between 50 and 200 μm.

### 2.3. NMR

All NMR experiments were performed on a Bruker AVANCE III NMR spectrometer at a $^1$H Larmor frequency of 400 MHz (9.4 Tesla). The stray field diffusion NMR experiments were performed on two commercial NMR probes, a 4 mm magic angle spinning (MAS) probe with a gradient coil under non-spinning conditions and a 5 mm diameter Bruker proton static probe. The pulsed field gradient diffusion experiments were performed using the Bruker 4 mm magic angle spinning probe with a 50 G/cm gradient capability. A pulsed field gradient stimulated echo sequence (PFG-STE) (Fig. 1a) was used [51]. The gradient pulse, $\delta$, was 2 ms, and the diffusion observation time, $\Delta$, was 1 s. A standard Bruker

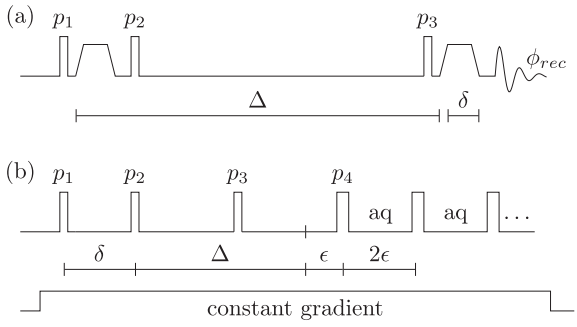


**Fig. 1.** (a) Pulsed-field stimulated echo pulse sequence with pulsed gradients of duration $\delta = 2$ ms and diffusion observation time $\Delta = 1$ s. (b) Stimulated echo pulse sequence with CPMG acquisition train under a constant magnetic stray field. $\delta$ varied from 60 to 350 μs. $\Delta$ was kept constant at 1 s. The echo delay $\epsilon$ was set to 100 μs. Pulses $p_1$ to $p_3$ are 90° pulses for both sequences and $p_4$ is a 180° pulse. The phase cycle for the pulse sequence (b) is as follows: $p_1$ (02)8 (13)8, $p_2$ (0022)4, $p_3$ (0)4 (2)4, $p_4$ (1)8 (3)8, aq (2002022013313 003) [56].

gradient shape file was used, SMSQ10.100, which is rectangular in shape with smoothed edges to give a gradient integral of 90% of a square pulse. The proton spin-lattice relaxation time ($T_1$) for the water in the foams and surrounding the polystyrene beads was measured using an inversion recovery experiment and found to be 3 s, therefore the recycle delay was set to 15 s. The gradient pulse was incremented from 2 to 90% in 32 increments. Sixteen scans were acquired for each increment.

For the stray field experiments, the NMR probe was lowered out of the magnet by 6–7 cm. At this position the resonance frequency was reduced by 0.5–1 MHz depending on the final position. The magnetic field gradient across the sample was calibrated using a water sample with a known free self-diffusion coefficient of $2.0 \times 10^{-9}$ m$^2$ s$^{-1}$ at 20 °C [52]. The magnetic field gradient ranged between 135 G/cm and 200 G/cm and was measured before each set of experiments during the study.

The magnetic field gradient across the sample is required to be constant. The linearity of the gradient is easily checked by performing a diffusion experiment on a sample of water with a known self-diffusion coefficient. The signal integral, $S$, is given by the following equation, $S = S_0 \exp(-D\Delta\delta^2\gamma^2 g^2)$, where $S_0$ is the signal integral for zero gradient encoding time, $D$ is the self diffusion coefficient, $\Delta$ is the diffusion observation time, $\delta$ is the gradient encoding time, $g$ is the gradient strength and $\gamma$ is the gyromagnetic ratio. For a linear gradient over the sample, a stimulated echo experiment should produce a straight line plot when the logarithm of $S/S_0$ is plotted against $\Delta q^2$, where $q = \delta\gamma g$ and has units of m$^{-1}$.

The stray field diffusion experiments were performed using a stimulated echo pulse sequence [51] with a Carr-Purcell-Meiboom-Gill (CPMG) [53,54] acquisition [55] (Fig. 1b). The 90° pulse width was set to 3.2 µs. The diffusion observation time, $\Delta$, was set to 1 s for the foams. The recycle delay was set to 6 s. In the initial experiments, the diffusion encoding time, $\delta$ was linearly incremented in 32 steps from 5 to 350 µs. A full 16 step phase cycle was used [56] giving an overall experimental time of 1 h. In later experiments, the number of acquisitions was reduced to 8 and the number of encoding steps reduced to 16 to give an experimental time of 15 min. The acquisition time echo window, $\epsilon$, for the CPMG sequence was set to 100 µs and 320 echoes were acquired during the acquisition resulting in a decay of the signal of approximately 30%. The spectral width was 1 MHz.

The stray-field diffusion data were processed in the time domain. The real and imaginary components of the FID were first phased to maximize the signal in the real channel. Each CPMG echo peak was isolated, keeping only the top 70% of the signal and summed together to give the final diffusion data. The position of the $q$-space maximum in the diffusion data was determined by an nth order polynomial fit over the relevant range. The value of $T_2$ was estimated by fitting an exponential to the CPMG echo train data. The processing software was written in the Python [57] programming language and used the scipy [58] and nmrglue [59] libraries to process and read in the NMR data. Example Python scripts in notebook form [60] and experimental data are provided in the supplementary data.

## 3. Results

### 3.1. Calibration of the stray-field gradient

Fig. 2 shows the stray field diffusion results for water in the 5 mm and 4 mm probes using the pulse sequence in Fig. 1b. In both cases, the data decrease linearly, indicating that the gradient across the sample is constant. The experiment shows a good dynamic range with little deviation from a straight line down to 2% in the case of the 4 mm sample. From these plots the magnetic field gradient across the sample can be calculated.

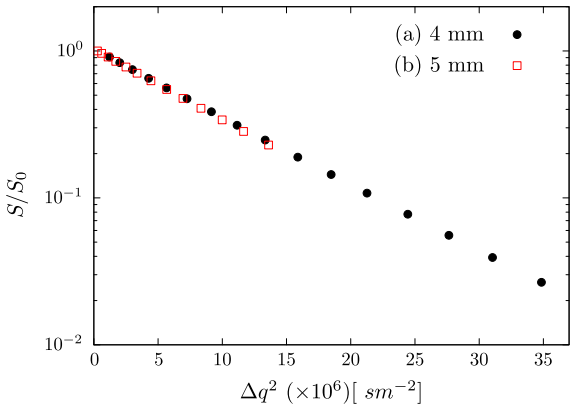


**Fig. 2.** Calibration of stray field gradient using a sample of water for two different NMR probes. (a) 4 mm probe, $\Delta$ = 100 ms, $\delta$ = 60–320 µs, gradient = 137 G/cm. (b) 5 mm probe, $\Delta$ = 80 ms, $\delta$ = 25–175 µs, gradient = 175 G/cm.

### 3.2. Stray field diffusion validation

The monodisperse polystyrene beads in water sample was used to develop and validate the stray field diffusion method in terms of $q$-space imaging. Fig. 3 shows the results of a PFG-STE experiment of the water surrounding the polystyrene beads using the 4 mm MAS probe with gradient on the 9.4 Tesla system. Two diffraction maxima are observed at q values of 20,000 and 35,000 m$^{-1}$. This corresponds to a spacing of 50 and 29 µm, giving a $\sqrt{3}$ relationship between the two, similar to that observed in emulsion systems [36]. The first maximum correlates well with the diameter of the monodisperse beads which is given as 49.5 ± 0.8 µm from the certified documentation accompanying the beads. The observation of two maxima is due to the low polydispersity of the standard sample and shows that the volume sample size is sufficient to give good statistics and even packing over the sample volume. The second trace in Fig. 3, is the result of the stray-field stimulated echo diffusion experiment on the polystyrene beads. Again, a diffraction maximum is observed, overlaying almost exactly with the pulsed-field gradient data.

When a foam sample is introduced, the line width of the water proton signal is of the order of 1700 Hz (Fig. 4a), much wider than

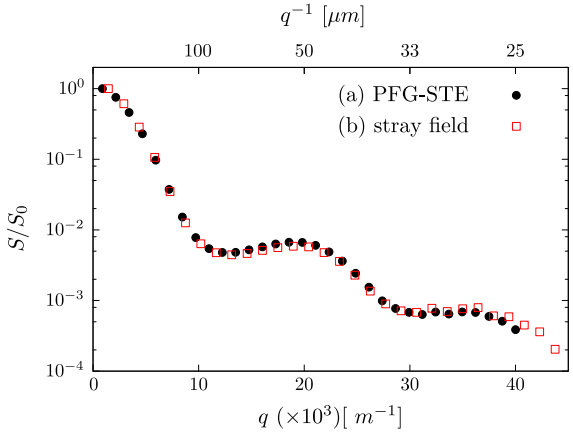


**Fig. 3.** Self-diffusion NMR experiment of water around 50 µm diameter monodisperse polystyrene beads on a 4 mm probe. (a) PFG-STE experiment. $\delta$ = 2 ms, $\Delta$ = 1 s. Maximum gradient strength = 50 G/cm. Gradient range from 2 to 90%. (b) Stray-field experiment. $\delta$ = 25–800 µs. $\Delta$ = 1 s. Stray-field gradient = 137 G/cm.

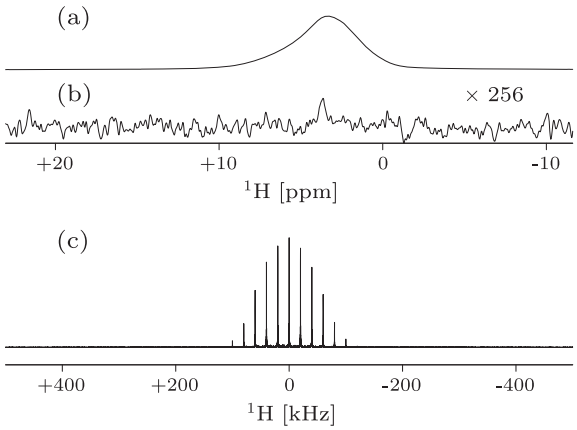


**Fig. 4.** $^1$H spectra (400 MHz) of a sample of monodisperse foam in 4 mm HRMAS insert for (a) a single pulse acquire experiment and (b) PFG-STE experiment with a gradient pulse, $\delta$ = 2 ms, gradient stabilisation delay of 1 ms, diffusion observation delay, $\Delta$ = 1 s and a gradient strength set to 2%, (c) Fourier transform of the CPMG echo train of a stray-field diffusion experiment with $\delta$ set to 25 µs, $\Delta$ = 1 s, CPMG echo spacing, $\epsilon$ = 100 µs. The stray-field gradient was 165 G/cm.

the signal arising from the water surrounding the polystyrene beads (33 Hz, data not shown). Therefore, when the PFG-STE experiment is performed under the same conditions, no signal is observed, even for the lowest gradient pulse setting (Fig. 4b) due to the loss of signal during the 3 ms gradient encoding time due to diffusion in the internal gradients present in the foam arising from the susceptibility mismatch. When the stray field diffusion experiment is applied to a monodisperse foam the outcome is more successful. Due to the short gradient encoding time, ranging from 25 to 600 µs a signal is recovered (Fig. 4c) that is modulated by the diffusion properties of the water in the system.

Fig. 5 shows the diffusion decay of the water in foams contained in a 5 mm and 4 mm outer diameter sample holder using different NMR probes. The experiments were performed within an hour of the samples being made. Diffraction maxima are observed in the signal decay for both samples, indicating that the foam has a low polydispersity and is stable for the duration of the experiment. The first diffraction peak indicates that the bubble diameter is of the order of 59 and 66 µm for the 4 and 5 mm samples respectively.

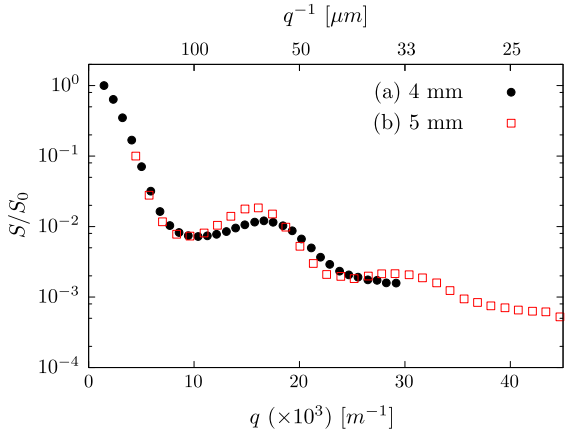


**Fig. 5.** Stray-field stimulated echo CPMG acquisition diffusion $q$-space NMR of two monodisperse foam. (a) 4 mm HR-MAS rotor. $\delta$ = 25–500 µs. $\Delta$ = 1 s. Stray-field gradient = 137 G/cm. (b) 5 mm NMR tube. $\delta$ = 60–600 µs. $\Delta$ = 1 s. Stray-field gradient = 175 G/cm.

### 3.3. Coarsening of foam with time

The stability of the foam was followed over time by performing the stray-field diffusion experiment repeatedly. In order to have a reasonable time resolution the number of gradient encoding steps was set to 16 and the number of scans at each point set to 8. With a recycle delay of 6 s, the experimental time was 15 min. Fig. 6 shows a stacked plot of the diffusion data for a foam sample in a 5 mm diameter cut-off NMR tube, placed horizontally in the 9.4 Tesla magnetic field. The initial diameter of the bubbles is 53 µm. The data is offset with the earliest experiment at the bottom of the figure. The diffraction peak is clearly observed at a $q$ value of 18 $\times 10^3$ m$^{-1}$. In the early stages of the experiment the plots do not change, indicating that the foam is stable in terms of bubble size and polydispersity. After approximately 4 h the diffusion plots begin to change. The peak maximum moves to smaller $q$ values and the peak becomes less pronounced. At this stage the experiment is showing that the bubbles are becoming larger and that the polydispersity of the foam is increasing. However, as the bubbles in the foam increase in size the diffusion observation time of the experiment is fixed at 1 s, therefore the diffusion time is no longer optimal for the increasing size of the bubbles. This will also affect the definition of the diffraction peak to some degree.

An estimate of the bubble diameter can be obtained from the data in Fig. 6 by plotting the $1/q$ values at the peak maximum as a function of time. The results for three different initial diameter foams are plotted in Fig. 7a with their properties in terms of bubble diameter and water content given in Table 1. The discrepancy between the microscopy and diffusion diameter values is quite large with the microscopy values being always bigger. This is probably due to the expansion of the bubbles when exposed to air due to the presence of the perfluorohexane creating a large osmotic imbalance. The NMR samples are sealed and are collected in a manner that minimises exposure to air.

All three foams show a stable period where the foam size does not change. This period of time increases with initial bubble diameter size. The lack of noise in the figure during this time period is due to the fact the diffusion data perfectly overlap as can be seen from Fig. 6. The bubble diameter eventually starts to change for all three foams, increasing in size. At longer times it becomes increasingly difficult to judge where the maximum is in the plots, hence the scatter in the data.

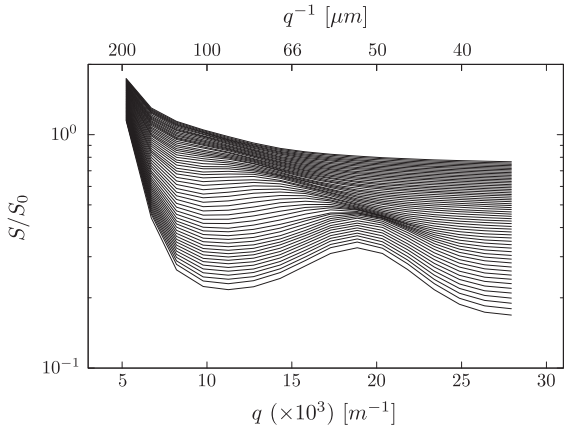


**Fig. 6.** $q$-space diffusion data over time for a monodisperse foam sample in a 5 mm NMR tube. Each experimental data set took 15 min to acquire. The foam was monitored for 15 h with the diffraction peak discernible for 8 h. The first acquired data set is at the bottom of the stacked plot. $\delta$ = 60–320 µs. $\Delta$ = 1 s. Stray-field gradient = 175 G/cm.

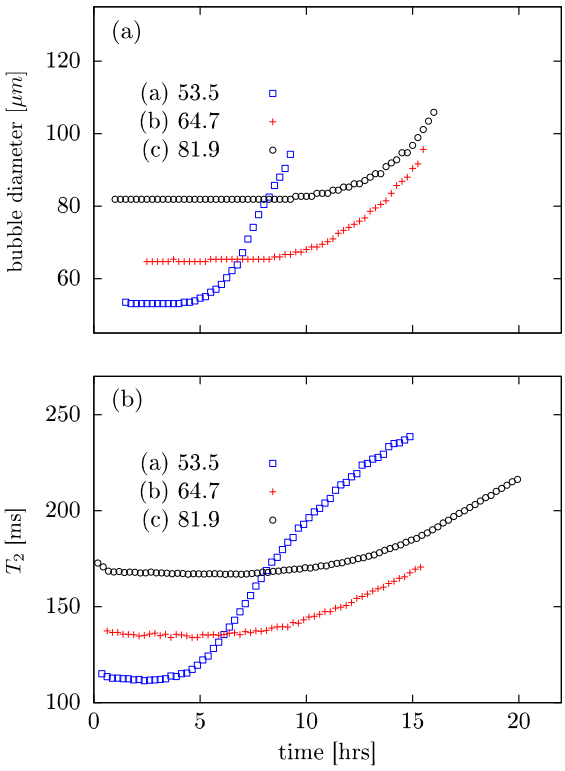


**Fig. 7.** Stability of foam based on the $q$-space diffusion NMR data (a) and the $T_2$ relaxation data (b) for three different initial diameter monodisperse foams. The legend gives the size of bubbles in μm.

**Table 1**
Diameter of three foams in microns from microscopy and diffusion NMR together with initial water volume fraction used in the stability studies.

| Foam | Microscopy | Diffusion NMR | Water fraction |
|---|---|---|---|
| (a) | 66 | 53.5 | 0.33 |
| (b) | 80 | 64.7 | 0.25 |
| (c) | 90 | 81.9 | 0.33 |

All three foams show a stable period where the diffraction maximum does not change. The duration of the stable period increases with the initial bubble diameter size. Eventually the diffraction maximum starts to change position for all three foams, shifting towards higher $q$ values.

The stability of the foams can also be followed by measuring the apparent $T_2$ of water signal from the CPMG echo train. This analysis is summarized in Fig. 7b. The relaxation rate for the first diffusion point is plotted against time. The graph shows that the initial $T_2$ values correlate well with the bubble size as each foam sample starts off at different $T_2$ values. There is an initial period of time when the $T_2$ values are constant. The length of this time period correlates well with the initial bubble diameter and then eventually the $T_2$ values start to increase as the foams evolve. The time period when the $T_2$ is constant matches the same time period over which the $q$-space diffraction data remain constant.

Fig. 8 plots the $T_2$ relaxation values for the three foams against the bubble diameter of the foam derived from the $q$-space imaging data. A linear correlation is observed and the parameters of the fit are used to correlate the $T_2$ relaxation data to a bubble size as the foam coarsens.

In Fig. 9 the diffusion and $T_2$ relaxation data are plotted again, to observe the scaling properties of the foam coarsening. On the log-log plot, the y-axis is the ratio of the derived bubble diameter as a

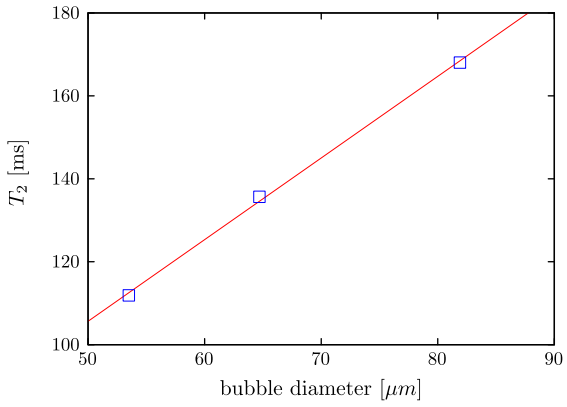


**Fig. 8.** Correlation between $T_2$ relaxation values for the three foams with the bubble diameter derived from the $q$-space peak maximum.

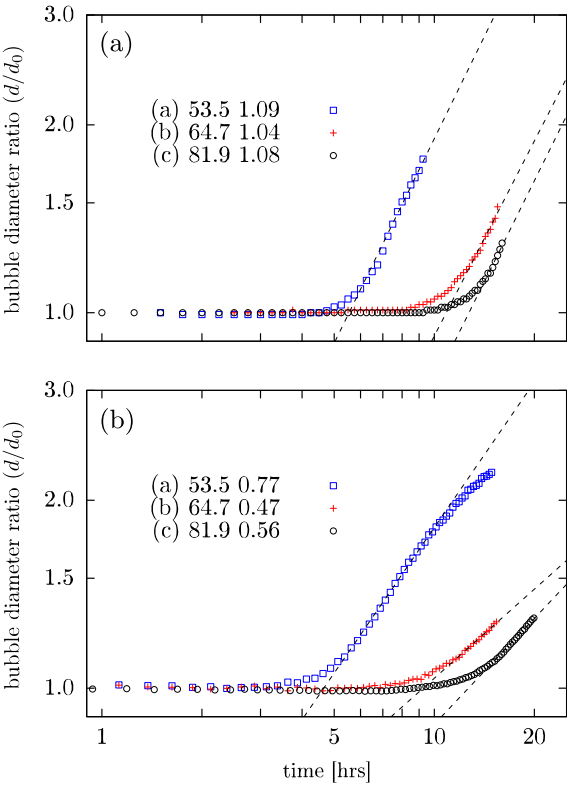


**Fig. 9.** Estimation of the power law coarsening dynamics for three foams of different initial diameters (53.5–81.9 μm) derived from $q$-space imaging data (a) and the $T_2$ relaxation data (b). The relaxation data has been converted to bubble diameter using the parameters derived from the straight line fit in Fig. 8 the values obtained for the slopes are given in the legends together with the initial bubble diameter.

function of time to the initial bubble diameter. The x-axis corresponds to the evolution time in hours. In the literature, for this axis a ratio is sometimes taken using a characteristic diffusion time [42]. However, we have chosen to use a simple time axis, following Isert [7], as both approaches gave very similar results given the uncertainty in defining the slope. In the plots an attempt is made to calculate the power-law exponent value when the foam starts to destabilise. The slopes obtained for all three foams are close to a value of 1 for the $q$-space diffusion data (Fig. 9a). For the data derived from the relaxation analysis the slopes vary between 0.77 and 0.47. The values obtained are very much dependent on

the fitting region used and therefore they have a large error associated with them.

## 4. Discussion

The results of the stray-field diffusion measurements show that the technique can be applied to foams without the need for chemical modification to reduce the susceptibility differences. By employing monodisperse foam, the diffusion experiments provide a simple way to follow the stability of the foams by tracking the position of the $q$-space maximum. The stability of the aqueous foams follow the expected trend in terms of bubble size.

Foams with bigger initial bubbles sizes are more stable due to the overall lower Laplace pressure. The stability increase will also be due to the relative smaller differences in Laplace pressure between bubbles for the foams with bigger initial bubble sizes. The microfluidic system produces bubbles with a certain polydispersity which will be dependent on the operating conditions. It is expected, in the microfluidic system that the relative polydispersity of the foam will increase as the bubble size decreases due to the increased effect of fluctuations in the pumping system. This increased initial polydispersity for foams of smaller initial bubble size will reduce the stability of such foams even further.

A feature of the foam stability experiments, upon the addition of the perfluorohexane gas, is the long period where the NMR data remains constant. Without the gas, the stability of the foams are on the order of a few minutes. During this period the bubble size remains constant based on the interpretation of the diffusion and $T_2$ data. From the experiments it is not clear if the onset of coarsening is due to some drainage minimum being reached. Simple single pulse experiments would show the presence of drained water, but this would mean interleaving the experiments with the diffusion experiments and involve manually, repositioning and retuning the probe for each experiment, therefore this was not done. The $T_2$ experiments as well as being sensitive to the size of the bubbles will also be impacted by drainage due to the presence of drained free water not associated with the foam. This will be seen in an increase in the $T_2$ values. In the stable period, there is little evidence of this occurring as the $T_2$ values remain constant.

At long times, dry and wet foams, coarsening solely to Laplace pressure differences, are expected to reach an asymptotic growth rate that is indicative of the type of diffusion mechanism present in the foam. The bubble size distribution of the foam as a function of time is also expected to reach a self-similar growth regime. A number of authors have shown evidence of this behaviour in foams [7,14,15,42,61]. Isert et al. [7] with their work under microgravity conditions have shown that there is a transition between the two diffusion mechanisms as a function of water content. They showed that the cross over between direct diffusion for dry foams, to diffusive diffusion for wet foams occurred over the water fraction range of 0.20–0.38.

In the three foam samples we have investigated the slopes of the coarsening behaviour were all close to a value of 1 for the diffusion data and between 0.77 and 0.45 for the relaxation data rates than between 0.33 and 0.5 expected for coarsening being the dominating mechanism and that they have reached a self-similar scaling regime given the water content of the foams.

The relaxation data values are a result of a weighted average of the bubble distribution in the foam. The diffusion value for the bubble size is taken from the $q$-space maximum. The width of the peak should be related to polydispersity, while the actual maximum should be indicative of the volume-averaged bubble diameter. As the foam ages, and becomes increasingly polydisperse the NMR diffusion experiment becomes less sensitive to the foam structure as the diffraction maxima becomes more poorly defined. In previous studies of $q$-space imaging on model monodisperse polystyrene beads systems the diffusion data was analysed using a pore-glass hopping model to give the size of the polystyrene beads and an estimate of the polydispersity present [31,33]. In this model a number of assumptions are required for it to hold; the spheres are packed randomly, the dimensions of the spaces between the beads where the water resides is small compared to the diameter of the beads and there is a separation of timescales for diffusion within pores and between pores. In monodisperse aqueous foams it is beyond the scope of this paper to validate all of the key assumptions required to use this model, but it is clear that the packing of the monodispersed aqueous foams is ordered [41,43], therefore a key aspect of the model is invalid and the analysis of the diffusion data in this manner was not pursued.

Both sets of values are too high for a foam undergoing only coarsening in the self-similar regime. It may be that the self-similar regime is not reached. The foams start off essentially monodisperse and when they begin to coarsen the shape of the size distribution of the bubbles is expected to change as the foam becomes more polydisperse. At the stage where changes in the size distribution becomes self-similar, the diffusion experiment may no longer show any diffraction maximum. Another factor is that drainage may be occurring also as the foam shows signs of coarsening and this may increase the rate at which the bubbles coarsen. Warren [16] has shown that the bubble coarsening rate can be greater than 0.5 when other hydrodynamic regimes are present. The highest values obtained from the relaxation regime fall into this range and therefore the coarsening dynamics may not be as simple as one had expected.

## 5. Conclusions

The stray-field diffusion approach was able to measure the diffusion properties of the water in the foam whereas the pulsed field gradient diffusion approach failed. The loss of chemical shift resolution in the stray-field experiment, which is normally a major drawback for this technique is not an issue due to the inherent NMR properties of the foams which produce a broad single resonance in single pulse experiments.

The use of monodisperse foam makes the diffusion experiment useful and the results easy to interpret when following the stability of the foam. The NMR results have shown that the stability of the monodisperse foam is dependent on the initial bubble size and that rate of coarsening would appear to be linked to the initial size of the bubbles. In these studies, with the limited number of samples investigated in terms of bubble size and volume fraction, a link between the air/water fraction and the coarsening rate could not be established. Therefore, future work will focus on improving the robustness of the foam production and preparation of the NMR sample.

There is an issue with the duration of the diffusion experiment. The foams required the use of trace amounts of an inert insoluble gas to increase their stability. In the study the minimum time required for a diffusion experiment was 15 min. This could be reduced further to under 5 min by reducing the number of repetitions to two and decreasing the echo spacing of the CPMG acquisition train together with increasing the number of CPMG echoes to increase the signal to noise ratio. Moreover, there are a number of rapid diffusion experiments [62–64] that may be suitable for use with the stray-field approach and in future work these will be investigated. Finally, the technique should be suitable for investigating foams under dynamic conditions [65], such as flow in different sample geometries so that the rheology [66] of the foam may be probed.

## Acknowledgements

This work was carried out under EPSRC contract number 01SSN01112011.

## Appendix A. Supplementary material

Supplementary data associated with this article can be found, in the online version, at http://dx.doi.org/10.1016/j.jcis.2016.04.053.

## References

[1] M. Lee, E.Y. Lee, D. Lee, B.J. Park, Stabilization and fabrication of microbubbles: applications for medical purposes and functional materials, Soft Matter 11 (2015) 2067–2079.
[2] E. Rio, W. Drenckhan, A. Salonen, D. Langevin, Unusually stable liquid foams, Adv. Colloid Interf. Sci. 205 (2014) 74–86.
[3] B.S. Murray, Stabilization of bubbles and foams, Curr. Opin. Colloid Interf. Sci. 12 (2007) 232–241.
[4] W. Drenckhan, D. Langevin, Monodisperse foams in one to three dimensions, Curr. Opin. Colloid Interf. Sci. 15 (2010) 341–358.
[5] L. Saulnier, W. Drenckhan, P.-E. Larr, C. Angladea, D. Langevin, E. Janiaud, E. Rio, In situ measurement of the permeability of foam films using quasi-two-dimensional foams, Colloids Surf. A: Physicochem. Eng. Aspects 473 (2015) 32–39.
[6] J. Duplat, B. Bossa, E. Villermaux, On two-dimensional foam ageing, J. Fluid Mech. 673 (2011) 147–179.
[7] N. Isert, G. Maret, C. Aegerter, Coarsening dynamics of three-dimensional levitated foams: from wet to dry, Eur. Phys. J. E 36 (2013) 1–6.
[8] N. Isert, G. Maret, C.M. Aegerter, Studying foam dynamics in levitated, dry and wet foams using diffusing wave spectroscopy, Colloids Surf. A: Physicochem. Eng. Aspects 473 (2015) 40–45.
[9] D. Weaire, S. Hutzler, The Physics of Foams, Clarendon Press, Oxford, 1999.
[10] J. von Neumann, Metal Interfaces, vol. 108, American Society for Metals, Cleveland, 1952.
[11] J.A. Glazier, S.P. Gross, J. Stavans, Dynamics of two-dimensional soap froths, Phys. Rev. A 36 (1987) 306–312.
[12] J. Stavans, J.A. Glazier, Soap froth revisited – dynamic scaling in the two-dimensional froth, Phys. Rev. Lett. 62 (1989) 1318–1321.
[13] R.D. MacPherson, D.J. Srolovitz, The von Neumann relation generalized to coarsening of three-dimensional microstructures, Nature 446 (2007) 1053–1055.
[14] J. Lambert, I. Cantat, R. Delannay, R. Mokso, P. Cloetens, J.A. Glazier, F. Graner, Experimental growth law for bubbles in a moderately wet 3D liquid foam, Phys. Rev. Lett. 99 (2007) 058304-1–058304-4.
[15] J. Lambert, R. Mokso, I. Cantat, P. Cloetens, J.A. Glazier, F. Graner, R. Delannay, Coarsening foams robustly reach a self-similar growth regime, Phys. Rev. Lett. 104 (2010) 248304-1–248304-4.
[16] P.B. Warren, Hydrodynamic bubble coarsening in off-critical vapor-liquid phase separation, Phys. Rev. Lett. 87 (22) (2001) 225702-1–225702-4.
[17] M.J. McCarthy, Interpretation of the magnetic resonance-imaging signal from a foam, AIChE J. 36 (1990) 287–290.
[18] R. Assink, A. Caprihan, E. Fukushima, Density profiles of a draining foam by nuclear magnetic-resonance imaging, AIChE J. 34 (1988) 2077–2079.
[19] B.A. Prause, J.A. Glazier, S.J. Gravina, C.D. Montemagno, Three-dimensional magnetic resonance imaging of a liquid foam, J. Phys.: Condens. Matter 7 (1995) L511–L516.
[20] C.P. Gonatas, J.S. Leigh, A.G. Yodh, J.A. Glazier, B.A. Prause, Magnetic resonance images of coarsening inside a foam, Phys. Rev. Lett. 75 (1995) 573–576.
[21] D. Holland, A. Blake, A. Tayler, A. Sederman, L. Gladden, A Bayesian approach to characterising multi-phase flows using magnetic resonance: application to bubble flows, J. Magnet. Reson. 209 (2011) 83–87.
[22] D. Holland, A. Blake, A. Tayler, A. Sederman, L. Gladden, Bubble size measurement using Bayesian magnetic resonance, Chem. Eng. Sci. 84 (2012) 735–745.
[23] K. Ziovas, A. Sederman, C. Gehin-Delval, D. Gunes, E. Hughes, M. Mantle, Rapid sphere sizing using a Bayesian analysis of reciprocal space imaging data, J. Colloid Interf. Sci. 462 (2016) 110–122.
[24] S. Baete, Y.D. Deene, B. Masschaele, W.D. Neve, Microstructural analysis of foam by use of NMR R2 dispersion, J. Magnet. Reson. 193 (2008) 286–296.
[25] F.T. Kurz1, T. Kampf, L.R. Buschle, H.-P. Schlemmer, S. Heiland, M. Bendszus, C. H. Ziener, Microstructural analysis of peripheral lung tissue through CPMG inter-echo time R2 dispersion, PLoS ONE 10 (11) (2015) 1–22.
[26] R. Kleinberg, W. Kenyon, P. Mitra, Mechanism of {NMR} relaxation of fluids in rock, J. Magnet. Reson., Ser. A 108 (2) (1994) 206–214.
[27] L. Latour, P. Mitra, R. Kleinberg, C. Sotak, Time-dependent diffusion coefficient of fluids in porous media as a probe of surface-to-volume ratio, J. Magnet. Reson., Ser. A 101 (3) (1993) 342–346.
[28] R. Kleinberg, M. Horsfield, Transverse relaxation processes in porous sedimentary rock, J. Magnet. Reson. 88 (1) (1990) 9–19 (1969).
[29] M.L. Johns, K.G. Hollingsworth, Characterisation of emulsion systems using NMR and MRI, Prog. NMR Spectrosc. 50 (2007) 51–70.
[30] P. Stevenson, A.J. Sederman, M.D. Mantle, X. Li, L.F. Gladden, Measurement of bubble size distribution in a gas-liquid foam using pulsed-field gradient nuclear magnetic resonance, J. Colloid Interf. Sci. 352 (2010) 114–120.
[31] P.T. Callaghan, A. Coy, D. MacGowan, K.J. Packer, F.O. Zelaya, Diffraction-like effects in NMR diffusion studies of fluids in porous solids, Nature 351 (1991) 467–469.
[32] P.T. Callaghan, S.L. Codd, J.D. Seymour, Spatial coherence phenomena arising from translational spin motion in gradient spin echo experiments, Concepts Magnet. Reson. 11 (4) (1999) 181–202.
[33] P.T. Callaghan, A. Coy, T.P.J. Halpin, D. MacGowan, K.J. Packer, F.O. Zelaya, Diffusion in porous systems and the influence of pore mophology in pulsed gradient spin-echo nuclear magnetic resonance studies, J. Chem. Phys. 97 (1) (1992) 651–662.
[34] P. Kuchel, A. Coy, P. Stilbs, NMR diffusion-diffraction of water revealing alignment of erythrocytes in a magnetic field and their dimensions and membrane transport characteristics, Magnet. Reson. Med. 37 (1997) 637–643.
[35] B. Balinov, O. Söderman, J.C. Ravey, Diffraction-like effects observed in the PGSE experiment when applied to a highly concentrated water/oil emulsion, J. Phys. Chem. 98 (1994) 393–395.
[36] B. Håkansson, R. Pons, O. Söderman, Structure determination of a highly concentrated w/o emulsion using pulsed-field-gradient spin-echo nuclear magnetic resonance diffusion diffractograms, Langmuir 15 (1999) 988–991.
[37] D. Topgaard, C. Malmbourg, O. Söderman, Restricted self-diffusion of water in a highly concentrated w/o emulsion studied using modulated gradient spin-echo NMR, J. Magnet. Reson. 156 (2002) 195–201.
[38] A. Woodward, T. Cosgrove, J. Espidel, P. Jenkins, N. Shaw, Monodisperse emulsions from a microfluidic device, characterised by diffusion NMR, Soft Matter 3 (2007) 627–633.
[39] A.I. Romoscanu, A. Fenollosa, S. Acquistapace, D.G.T. Martins-Deuchande, P. Clausen, R. Mezzenga, M. Nyden, K. Zick, E. Hughes, Structure, diffusion, and permeability of protein-stabilized monodispersed oil in water emulsions and their gels: a self-diffusion NMR study, Langmuir 26 (9) (2010) 6184–6192.
[40] E. Hughes, A.A. Maan, S. Acquistapace, A. Burbidge, M.L. Johns, D.Z. Gunes, P. Clausen, A. Syrbe, J. Hugo, K. Schroen, V. Miralles, T. Atkins, R. Gray, P. Homewood, K. Zick, Microfluidic preparation and self diffusion PFG-NMR analysis of monodisperse water-in-oil-in-water double emulsions, J. Colloid Interf. Sci. 389 (2013) 147–156.
[41] D. Weaire, R. Phelan, The structure of monodisperse foam, Philos. Magaz. Lett. 70 (1994) 345–350.
[42] A.M. Ganan-Calvo, J.M. Fernandez, A.M. Oliver, Coarsening of monodisperse wet microfoams, Appl. Phys. Lett. 84 (2004) 4989–4991.
[43] A.J. Meagher, M. Mukherjee, D. Weaire, S. Hutzler, J. Banhart, F. Garcia-Moreno, Analysis of the internal structure of monodisperse liquid foams by X-ray tomography, Soft Matter 21 (2011) 9881–9885.
[44] E.G. Schutt, D.H. Klein, R.M. Mattrey, J.G. Riess, Injectable microbubbles as contrast agents for diagnostic ultrasound imaging: the key role of perfluorochemicals, Angew. Chem. Int. Ed. 42 (2003) 3218–3235.
[45] M. Cifelli, A practical tutorial to set up NMR diffusometry equipment: application to liquid crystals, Magnet. Reson. Chem. 52 (2014) 640–648.
[46] R. Kimmich, W. Unrath, G. Schnur, E. Rommel, NMR measurement of small self-diffusion coefficients in the fringe field of superconducting magnets, J. Magnet. Reson. 91 (1991) 136–140.
[47] D.G. Rata, F. Casanova, J. Perlo, D.E. Demco, B. Blümich, Self-diffusion measurements by a mobile single-sided NMR sensor with improved magnetic field gradient, J. Magnet. Reson. 180 (2006) 229–235.
[48] A. Samoilenko, D. Artemov, L. Sibel'dina, Formation of sensitive layer in experiments on NMR subsurface imaging of solids, Jetp Lett. 47 (1988) 417–419.
[49] J. Mitchell, P. Blümler, P. McDonald, Spatially resolved nuclear magnetic resonance studies of planar samples, Prog. Nucl. Magnet. Reson. Spectrosc. 48 (2006) 161–181.
[50] B.R. Benson, H.A. Stone, R.K. Prud'homme, An off-the-shelf capillary microfluidic device that enables tuning of the droplet breakup regime at constant flow rates, Lab on a Chip 13 (2013) 4507–4511.
[51] J.E. Tanner, Use of the stimulated echo in NMR diffusion studies, J. Chem. Phys. 52 (1970) 2523–2526.
[52] M. Holz, S.R. Heil, A. Sacco, Temperature-dependent self-diffusion coefficients of water and six selected molecular liquids for calibration in accurate $^{1}$H NMR PFG measurements, Phys. Chem. Chem. Phys. 2 (2000) 4740–4742.
[53] H.Y. Carr, E.M. Purcell, Effects of diffusion on free precession in nuclear magnetic resonance experiments, Phys. Rev. 94 (3) (1954) 630–638.
[54] S. Meiboom, D. Gill, Modified spin echo method for measuring nuclear relaxation times, Rev. Scient. Instrum. 29 (1958) 688–691.
[55] M. Hürlimann, L. Venkataramanan, Quantitative measurement of two-dimensional distribution functions of diffusion and relaxation in grossly inhomogeneous fields, J. Magnet. Reson. 157 (2002) 31–42.
[56] F. Casanova, J. Perlo, B. Blümich (Eds.), Single-Sided NMR, Springer, 2011.
[57] E. Jones, T. Oliphant, P. Peterson, et al., SciPy: Open Source Scientific Tools for Python, 2001. <http://www.scipy.org/>.
[58] [link]. http://www.python.org/.
[59] J. Helmus, C. Jaroniec, NMRglue: an open source python package for the analysis of multidimensional NMR data, J. Biomol. NMR 55 (2013) 355–367.
[60] F. Pérez, B.E. Granger, IPython: a system for interactive scientific computing, Comput. Sci. Eng. 9 (3) (2007) 21–29, http://dx.doi.org/10.1109/MCSE.2007.53. <http://ipython.org>.

[61] D.J. Durian, D.A. Weitz, D.J. Pine, Scaling behaviour in shaving cream, Phys. Rev. A 44 (1991) R7902–R7905.
[62] Y.-Q. Song, X. Tang, A one-shot method for measurement of diffusion, J. Magnet. Reson. 170 (2004) 136–148.
[63] Y.-Q. Song, Multiple modulation multiple echoes: a one-shot method, Magnet. Reson. Imag. 23 (2005) 301–303.
[64] K. Szutkowski, I. Furó, Effective and accurate single-shot NMR diffusion experiments based on magnetization grating, J. Magnet. Reson. 195 (2008) 123–128.
[65] U. Scheven, Stray field measurements of flow displacement distributions without pulsed field gradients, J. Magnet. Reson. 174 (2005) 338–342.
[66] T. Blythe, A. Sederman, J. Mitchell, E. Stitt, A. York, L. Gladden, Characterising the rheology of non-newtonian fluids using PFG-NMR and cumulant analysis, J. Magnet. Reson. 255 (2015) 122–131.